PROCEEDINGS, 43rd Workshop on Geothermal Reservoir Engineering
Stanford University, Stanford, California, February 12-14, 2018
SGP-TR-213

A New Conceptual Framework for the Deep Roots of Magma-Driven Geothermal Systems

Samuel Scott[1,2], Thomas Driesner[2], Philipp Weis[3]

[1] School of Science and Engineering, Reykjavik University, Menntavegur 1, IS-101 Reykjavik, Iceland
[2] Institute of Geochemistry and Petrology, Department of Earth Sciences, ETH Zurich, 8092 Zurich, Switzerland
[3] GFZ German Research Centre for Geosciences, Potsdam, Germany

samuels@ru.is

Keywords: Numerical modeling, fluid flow, supercritical, boiling, condensation, magmatic intrusions, permeability, saline

ABSTRACT

Recent developments in numerical simulation tools provide new insights into natural phenomena occurring in the deep roots of magma-driven geothermal systems, including the formation of supercritical geothermal resources, boiling and condensation processes, and the dynamics of heat transfer from intrusions. This contribution highlights several recent studies which employ the Complex Systems Modeling Platform (CSMP++) to investigate the thermo-hydraulic structure of high-enthalpy geothermal systems. CSMP++ is a C++ code library which uses unstructured meshes to represent complex, geologically realistic model geometries and features a highly modular structure that allows users to write modules for material properties (e.g., permeability as a function of temperature). The use of a control volume finite element method for solving the set of coupled equations governing heat and mass transport by fluid flow combined with a realistic description of fluid properties up to magmatic conditions (i.e., 1000 ºC, 500 MPa, and 0 to 100% NaCl) enables simulation of fluid flow near intrusions. The ability to include a transiently cooling magmatic heat source allows significantly improved methods of resource and sustainability assessment in high-enthalpy geothermal systems, and provides a virtual test bed to explore scenarios for supercritical resource exploitation. As an illustration of the robustness of model results, the simulations reproduce the measured characteristics of the IDDP-1 reservoir if basic geologic characteristics appropriate for the Krafla system are assumed for the model set-up. The dynamics of fluid flow and heat transfer near intrusions are significantly altered if the pore fluid consists of seawater rather than dilute meteoric water, due to the accumulation of dense, hypersaline brines upon boiling above the intrusion and the potential for the clogging of pore space by halite precipitation. However, heat transport by high-enthalpy vapor is maximized in saline systems if the intrusion is deeper than ~4 km, and condensation rather than boiling prevails near the intrusion.

1. INTRODUCTION

Most of the electricity harnessed from geothermal heat is generated from magma-driven high-enthalpy geothermal systems. Since the natural lifetime of a high-enthalpy geothermal system driven by a single magmatic intrusion is typically on the order of ~10^4 years (Cathles et al., 1997; Hayba and Ingebritsen, 1997), while large-scale power production from magma-driven geothermal systems has at most proceeded for decades, modern geothermal reservoir engineering assumes that a nearly steady, "natural state" of a given system can be established in a model and then used as a reference for evaluating and predicting changes to a reservoir during operation (O'Sullivan et al., 2001). In systems with long-term production histories, reservoir modelers integrate data from geological and geophysical studies with field measurements to calibrate inverse models with parameter estimation and history matching. However, geothermal reservoir engineers are also tasked to build preliminary models for systems with little or no development history (Pritchett, 2007). In such instances, a conceptual model describing the thermal and hydrological features of magma-driven geothermal systems is crucial to inform estimates of a field's potential electricity generation capacity and decision-making concerning the location and depth of exploration wells. These conceptual models are mainly supported by geophysical data (e.g. Cumming, 2016) and numerical reservoir simulation (Grant and Bixley, 2011).

However, in contrast to models of geothermal reservoirs under production, rather few studies have focused on how geological factors control the long-term, undisturbed evolution and structure of high-enthalpy geothermal systems. Early numerical simulations of hydrothermal convection around magmatic intrusions demonstrated that the system behavior and lifetime is strongly impacted by host rock permeability (Norton and Knight, 1977; Cathles, 1977). Subsequent studies included the full thermodynamics of boiling water to magmatic conditions and demonstrated that host rock permeability controls the development of boiling zones and the overall thermal structure of a system (Hayba and Ingebritsen, 1997). While the near-surface parts of systems remain at boiling conditions through the main and later parts of system evolution, there may be different plume geometries, deep thermal structures, and hydraulic behaviors depending on the host rock permeability and the stage in the system lifetime (Scott et al., 2016).

Recently, there has been increasing interest in targeting supercritical geothermal resources near intrusions due to the potential for much greater rates of electricity generation per well (Friðleifsson et al., 2014; Reinsch et al., 2017). Such resources were encountered in 2009-2011 when the Iceland Deep Drilling Project drilled into a magma chamber at 2.1 in Krafla, Iceland (Elders et al., 2014). Recent studies show how host rock permeability governs the spatial extent and thermal structure of such resources (Scott et al., 2015). While host rocks with permeability near 10^{-15} m^2 develop supercritical zones extending hundreds of meters above the intrusion, supercritical fluid flow is confined to a thin layer (10s of m) enveloping the intrusion in host rocks with a higher permeability of 10^{-14} m^2. Below a permeability of ~10^{-16} m^2, fluid advection is limited and heat transfer is dominated by thermal conduction through rock (Ingebritsen et al., 2006).

While the hydraulic behavior of systems containing meteoric-derived, dilute water can be approximated by models featuring pure H_2O as the pore fluid, several active high-enthalpy geothermal systems, such as Reykjanes in Iceland or Salton Sea in California feature geothermal waters containing significant concentrations of dissolved salt. Saline water phase relations, approximated by the system H_2O-NaCl, differ significantly from those of pure water, and liquid-vapor coexistence can extend to temperatures and pressures far above the critical values of pure water. Heating may gradually transform a cool saline liquid into a hot, vapor-like fluid or result in a hot, liquid-like phase, depending on pressure (Foustokous and Seyfried, 2007). Phase separation of a heated fluid may occur by condensation if pressure is higher than the critical pressure for the given salinity, or by boiling if pressure is lower (Fournier, 1987; Geiger et al., 2005). Depending on the dynamics of saline fluid phase separation, high-enthalpy vapor-like resources such as those presently being sought after by the IDDP-2 well in Reykjanes may develop to varying extents (Friðleifsson et al., 2017).

Here we report results from a series of studies (Scott et al., 2015, 2016, 2017) investigating aspects of hydrothermal convection around a transiently cooling magmatic intrusion. We describe key features of the natural – undisturbed by production – thermal and hydraulic structures of high-enthalpy systems and their evolution over the lifetime of a system. We explore the effects of host rock permeability, the emplacement depth and geometry of the intrusion, temperature-dependent permeability near the intrusion, and fluid salinity on the depth and extent of boiling zones, the thermal structure of supercritical geothermal resources, and the dynamics of fluid flow and heat transfer. We show how the thermal and hydraulic structures of high-enthalpy geothermal systems respond systematically to variation of these primary parameters over a relatively small range. Lastly, we condense these systematics to a set of key findings that may be useful in exploration and resource assessment.

2. METHODOLOGY

Convective circulation of groundwater above magmatic intrusions can be described with a continuum, porous medium approach based on Darcy's law. The governing equations of multi-phase mass and energy conservation are solved using a continuum porous media approach with a pressure-enthalpy-salinity-based formulation in a Control Volume-Finite Element Method numerical scheme using the Complex Systems Modeling Platform (CSMP++), which has been described in detail by Weis et al. (2014).

2.1 Numerical Method

Phase velocities were obtained using an extended two-phase (i = liquid, vapor) form of Darcy's law:

$$v_i = -k \frac{k_{r,i}}{\mu_i} (\nabla p - \rho_i g)$$

where k is the rock permeability, $k_{r,i}$ relative permeability of the fluid phase, μ_i dynamic viscosity, ∇p pressure gradient, ρ_i phase density, and g the gravitational acceleration vector. A linear relative permeability model with a liquid residual saturation of 0.3 and vapor residual saturation of zero is adopted (Hayba and Ingebritsen, 1997; Weis et al., 2014). The pore fluid consists of pure water, and all fluid properties correspond to Haar et al. (1984), and the effect of adding NaCl is described by Driesner and Heincrich (2007) and Driesner (2007).

Conservation of fluid mass is given by:

$$\frac{\partial\left(\phi(S_l\rho_l + S_v\rho_v + S_h\rho_h)\right)}{\partial t} = -\nabla\cdot(v_l\rho_l) - \nabla\cdot(v_v\rho_v) + Q_{H2O+NaCl}$$

Where the subscript h refers to the halite phase, ϕ is rock porosity, S_i is the volumetric saturation of each phase and $Q_{H2O+NaCl}$ is a fluid source term. Energy conservation accounts for conduction of heat in the rock and advection of enthalpy by fluid.

$$\frac{\partial\left((1-\phi)\rho_l h_r + \phi(S_l\rho_l h_l + S_v\rho_v h_v + S_h\rho_h h_h)\right)}{\partial t} = \nabla\cdot(K\nabla T) - \nabla\cdot(v_l\rho_l h_l) - \nabla\cdot(v_v\rho_v h_v) + Q_e$$

with K as the thermal conductivity of the rock and Q_e as an energy source term. Fluid and rock are assumed to be in local thermal equilibrium, and total enthalpy is distributed over fluid and rock contained in a control volume such that they are at the same temperature (Weis et al., 2014).

Conservation of salt mass is given by:

$$\frac{\partial\left(\phi(S_l\rho_l X_l + S_v\rho_v X_h + S_h\rho_h X_h)\right)}{\partial t} = -\nabla\cdot(v_l\rho_l X_l) - \nabla\cdot(v_v\rho_v X_l) + Q_{NaCl}$$

with X denoting the mass fraction of NaCl in the phase indicated and a source term Q_{NaCl}.

2.2 Model Set-up

A typical model configuration is given in Fig. 1, for an intrusion centered at 3 km depth with horizontal and vertical axis lengths of 2 km and 1 km, respectively. In this study, the term 'emplacement depth' refers to the depth to the top of the intrusion, and is thus 2 km for the example in Fig. 1. The computational domain is 5 km and 15 km in vertical and horizontal extent, respectively, and consists of roughly 14,000 elements. Initially, the porous medium is saturated with water and thermally equilibrates with a basal heat flux of 0.15 W m^{-2}. The

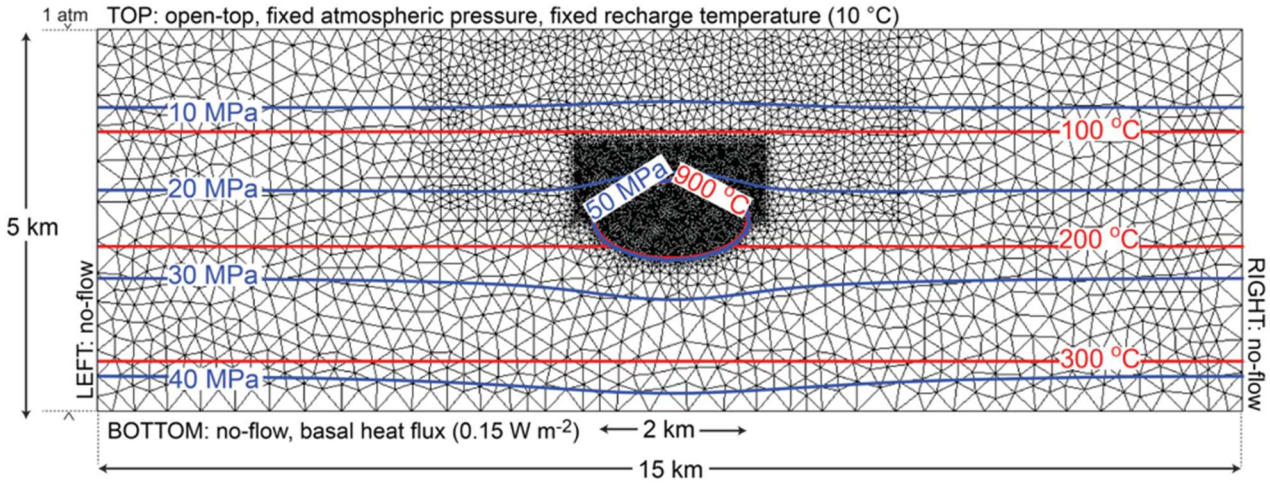

Figure 1. Model set-up and finite element grid for example simulation with intrusion emplacement depth of 2 km.

in
The top boundary is fixed at atmospheric pressure, and features a mixed energy boundary condition. In elements where volume flux is upward, fluids vent at temperatures of the ascending hydrothermal fluids; elements where the volume flux is downward take in fluid at a temperature of 10 ºC. This simulates the effect of recharge of cold meteoric water, sufficient to maintain a stable elevation of the water table. The other boundaries are no-flow boundaries, placed sufficiently far from the heat source that they do not affect fluid convection near the intrusion.

At the onset of simulation time, fluid within the pore space of the intrusion is set to a temperature of 900 °C and lithostatic pressure, describing an instantaneous intrusion of magma into the upper crust. Host rock permeability is homogenous and isotropic, and temperature-dependent near the intrusion. This temperature-dependent permeability is included to simulate the transition from advection- to conduction-dominated heat transfer around the intrusion, representing the brittle-ductile-transition (BDT). We adopt the formulation of Hayba and Ingebritsen (1997) where permeability decreases logarithmically with increasing temperature above a selected BDT temperature (T_{BDT}). While a T_{BDT} of 360 °C used by Hayba and Ingebritsen (1997) is appropriate for quartz-bearing rocks at normal crustal strain rates, a T_{BDT} of 450 or 550 °C may be more appropriate for basaltic rocks (Violay et al., 2015). The effect of latent heat of crystallization is taken into consideration with a temperature-dependent rock heat capacity, which doubles from 880 J kg^{-1} °C^{-1} at temperatures below 650 °C to 1760 J kg^{-1} °C^{-1} at temperatures greater than 700 °C.

3. RESULTS

In this contribution, we summarize findings described in detail in a series of recent publications (Scott et al., 2015, 2016, 2017), seeking to elucidate three main aspects of geothermal system behavior: i) the effect of primary geologic factors on large-scale thermal structure and temporal evolution of magma-driven geothermal systems, ii) the formation of supercritical geothermal resources near an intrusion, iii) how systems with seawater as the pore fluid develop different styles of phase separation and heat transfer dynamics.

3.1 Effect of Host Rock Permeability and Intrusion Depth on Geothermal System Structure and Temporal Evolution

Host rock permeability is a primary control on the general structure, temperature distribution, and extent of boiling zones in geothermal systems. Systems with high host rock permeability generally display near-isothermal upflow of single-phase liquid in their deeper parts and boiling in their shallow parts. Intermediate permeability systems can develop boiling zones extending from the surface to the top of the intrusion and, accordingly, show a temperature-depth distribution that tends to follow the boiling curve with depth. Intrusion depth is a major control on whether one or more spatially separated geothermal reservoirs form in the upper parts of a geothermal system driven by a single intrusive body.

For systems with high host-rock permeability and an intrusion emplacement depth of 2.5 km, two ~300 ºC liquid plumes develop rapidly after emplacement of the intrusion (Fig. 2a). The plumes reach the surface within 0.8 ky and merge to form a single upflow zone centered on the intrusion with a boiling zone at <1 km depth shaped like an inverted teardrop (Fig. 2b). A narrow (~100 m thick), nearly isothermal (300 ºC) liquid upflow zone underlies the center of the boiling zone. During the waning stage (after the heat source has cooled completely), boiling persists in the upper 0.5 km for 3–4 ka (Fig. 2c).

Fig. 2d–f depicts the evolution of a system with intermediate host rock permeability of 10^{-15} m^2 and emplacement depth of 2.5 km. Two boiling plumes with temperatures >300 ºC develop over the margins of the intrusion and reach the surface within 3 ka (Fig. 2d). The system is at main stage conditions with a boiling upflow extending from the surface to ca. 2.5 km depth (Fig. 2e). The width of the boiling upflow is nearly constant but increases in the near vicinity of the intrusion. After the intrusion cools, the depth of boiling decreases rapidly to ~1 km. However, the system cools from the bottom up throughout the waning stage, and the upper parts of the system appear like the main stage, with boiling persisting at the surface for ~5 ka (Fig. 2f).

While systems with a heat source located at 2.5 km depth normally develop single upflow plumes (e.g. Fig 2a-f), systems with a heat source located at 3 km depth (Fig. 2g-l) may develop multiple plumes that merge at depth as the system evolves. A system with an

emplacement depth of 3 km and a high host rock permeability develops two distinct plumes over the margins of the intrusion during the incipient stage (Fig. 2g). The plumes merge at depth after reaching the surface, but continue to diverge above 1.5 km depth into the pathways previously heated by the ascending plumes. A zone of downward-circulating cold (<200 ºC) water separates the two shallow boiling zones (Fig. 2h,i).

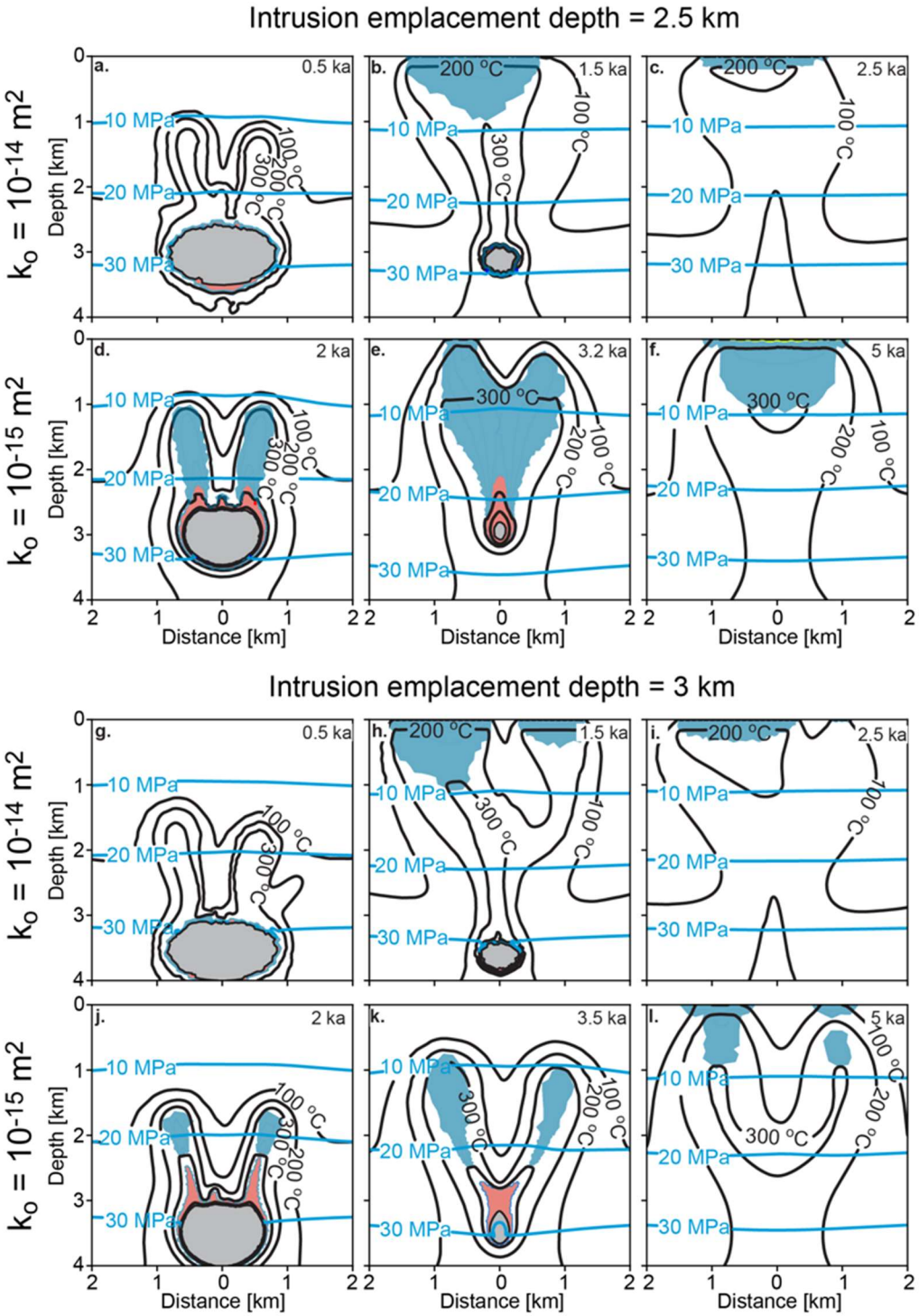

Figure 2: The temporal evolution of high-enthalpy geothermal systems under different conditions of host rock permeability (ko) and intrusion emplacement depth (defined as the initial depth to the top of the intrusion). Host rock permeability is set to 10^{-14} m² (a.-c., g.-i) or 10^{-15} m² (d.-f., j.-l.), and intrusion emplacement depth to 2.5 km (a.-f.) or 3 km (g.-l.). Temperature contours are shown with black lines, fluid pressure contours with blue lines). Zones of two-phase (liquid and vapor) coexistence are shown in blue, potentially exploitable supercritical water resources (see text) in red, and the impermeable intrusion in grey. Modified from Scott et al. (2016).

Multiple plumes also develop in a system with intermediate host rock permeability and at the same emplacement depth (Fig. 2j–l). As the system evolves, the plumes merge at the base, where a supercritical zone has formed centered on the intrusion (Fig. 2k). Because the thermal front must travel a greater distance upwards compared to the shallower intrusion, the intrusion cools below the brittle–ductile transition temperature before boiling occurs at the surface (~4 ka) (Fig. 2l).

3.2 Formation of Supercritical Geothermal Resources near Intrusions

A key control on the formation of supercritical resources are the conditions at which fluid circulation near an intrusion is cut off due to plastic deformation and closure of permeable flow paths. This can be approximated by the brittle-ductile transition temperature T_{BDT}, which can serve as a proxy for host rock lithology, as it ranges from ~360 ºC for silicic rocks at typical crustal strain rates (Fournier, 1999) to as high as 800 ºC for non-glassy basaltic rocks (Violay et al., 2015). Below a permeability of ~10^{-16} m^2, heat transport changes from being advection- to conduction-dominated (Ingebritsen et al., 2016), and any wells drilled into such conditions would encounter uneconomic rates of fluid production. Thus, the formation of potentially exploitable supercritical fluid resources hinges on whether hydrothermal fluid is heated to supercritical temperatures at conditions of sufficiently high rock permeability.

We define potentially exploitable supercritical resources as those parts of a geothermal system where permeability is >10^{-16} m^2 and temperature and specific enthalpy of water are greater than their critical values (373.976 ºC and 2.086 MJ kg^{-1} according to Haar et al., 1984). This definition avoids the distinction between 'superheated' (fluid pressure below the critical pressure) and 'supercritical' (above the critical pressure) resources, which is somewhat arbitrary as supercritical fluid properties vary gradually across the critical isobar. Rather, our definition allows analyzing the full continuum of supercritical resource conditions including the development of economically attractive resources at subcritical pressures, such as were encountered during drilling of the IDDP-1 well at Krafla.

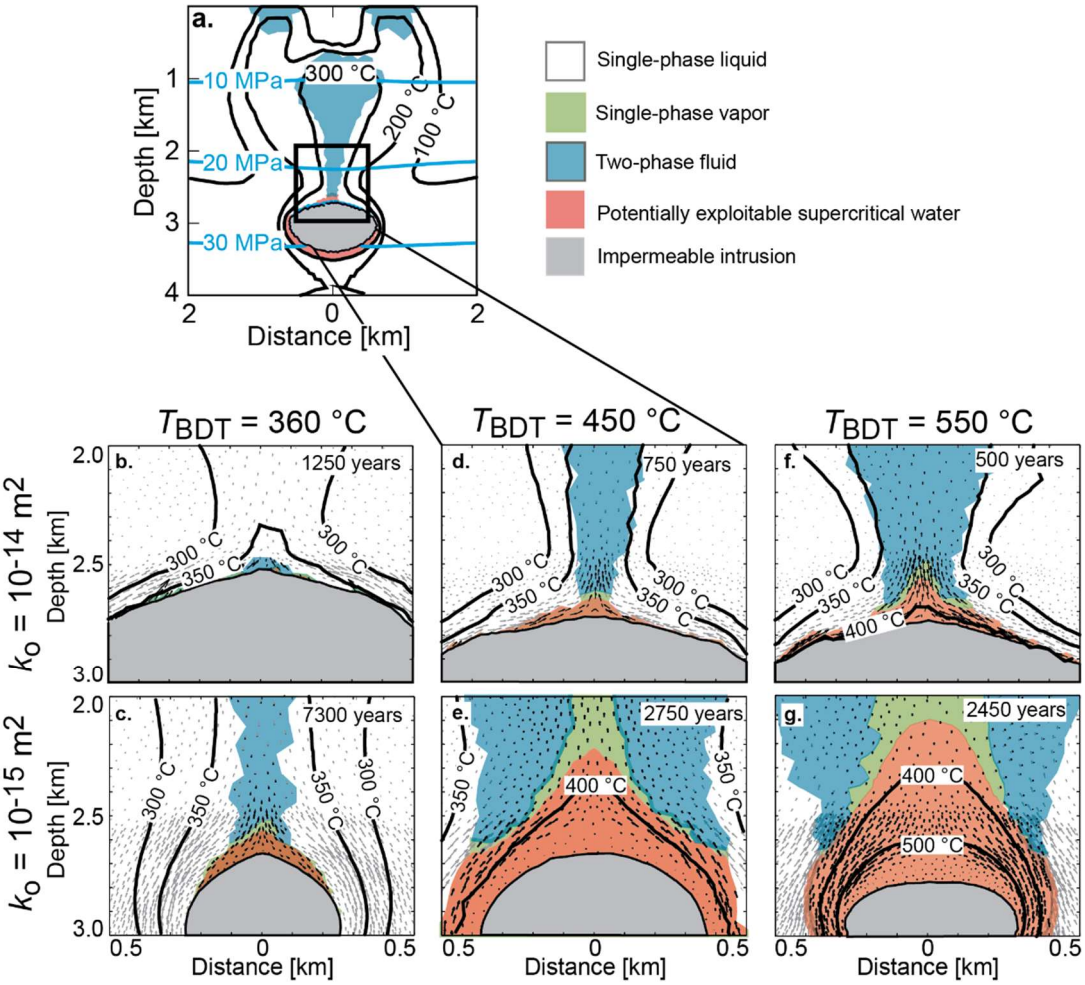

Figure 3: (a.) Typical large-scale thermal structure of a simulated geothermal system. The fluid phase state distribution and temperature/fluid pressure contours are shown with same color scheme as in Fig. 2. Zones of two-phase (liquid and vapor) coexistence are shown in blue, and single-phase vapor at a temperature below the critical temperature is shown in green. (b.-g.) Snapshots of the area near the top of the intrusion (black box in a), under different conditions of host rock permeability (k_o) and brittle–ductile transition temperature (T_{BDT}). Liquid (grey) and vapor (black) flow vectors are also shown (not to scale between different fluid phases or simulations). We vary k_o from 10^{-14} m^2 (b,d,f) to 10^{-15} m^2 (c,e,g) and vary T_{BDT} from 360 ºC (b,c), to 450 ºC (d,e), and 550 ºC (f,g). Modified from Scott et al. (2015).

Extensive supercritical water resources can develop if T_{BDT} is at least 450 ºC (Fig. 3d,e). Increasing T_{BDT} from 450 to 550 ºC results in somewhat larger supercritical zones without dramatically changing the thermo-hydraulic conditions of such reservoirs (Fig. 3f,g). For T_{BDT} of 360 ºC, (Fig. 3b,c) only minor supercritical resources develop because the threshold permeability is encountered at temperatures slightly higher than the critical temperature of water.

The extent and temperature of the supercritical resources strongly depend on host rock permeability. In high-permeability host rocks, the rate of convective water circulation surpasses the ability of the intrusion to heat most circulating water to supercritical temperatures, and supercritical water flow is confined to a thin (~10 m) boundary layer on the perimeter of the intrusion (Fig. 3d,f). Most of the supercritical resource only reaches temperatures of 375–400 ºC, where the thermodynamic ability of supercritical water to transport heat is maximized (Ingebritsen and Hayba, 1994; Jupp and Schultz, 2000), even if T_{BDT} is as high as 550 ºC. In contrast, supercritical resources in intermediate permeability systems are hotter (Fig. 3e,g). The water circulation rate near the intrusion is lower compared with high-permeability systems, so the conductive heat input across the brittle–ductile transition is sufficient to heat up a larger fraction of the circulating water to supercritical temperatures, and temperatures can approach T_{BDT} in the near vicinity of the intrusion. The supercritical resources can extend several hundred meters above the top of the intrusion.

3.3 Effect of Fluid Salinity on Geothermal System Thermal Structure

Under geothermal conditions, the system H_2O-NaCl (Driesner and Heinrich, 2007; Driesner, 2007) exhibits seven different combinations of the possible phase states vapor (V), liquid (L), and halite (H), as seen in Figure 4:

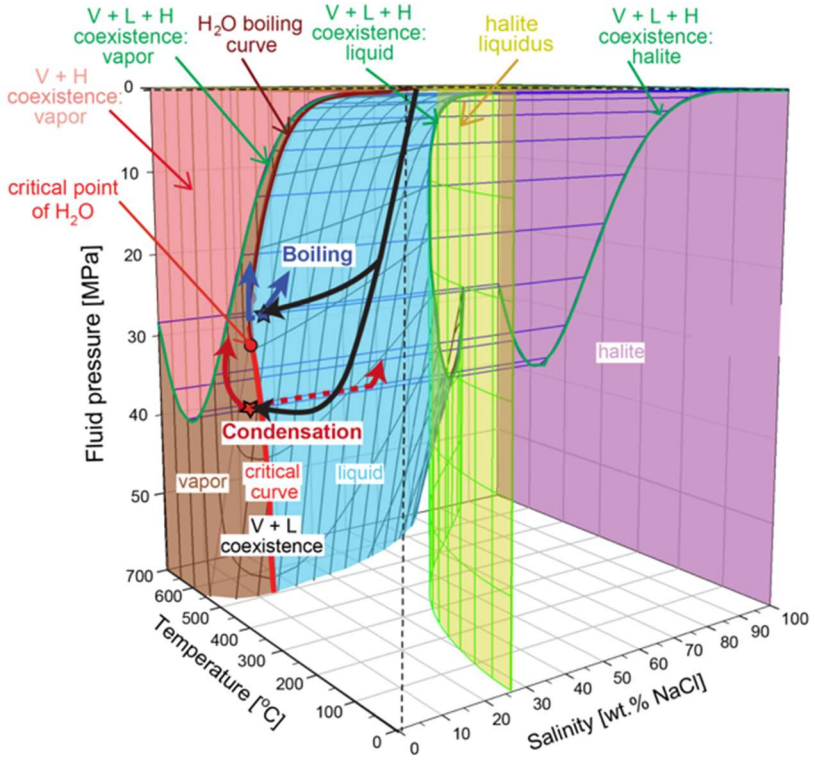

Figure 4: Phase diagram of the system H_2O-NaCl (Driesner and Heinrich, 2007) illustrating the effect of intrusion depth on the style of phase separation of an initial seawater-salinity fluid. The blue path represents the circulation from the surface to ~2.5 km depth, followed by upflow and boiling, while the orange path represents the circulation to ~4.5 km depth, followed by upflow and condensation. Modified from Scott et al. (2017).

1. V+L: The V+L surface describes the compositions of coexisting liquid and vapor at a given pressure and temperature. At temperatures below the critical temperature of pure water, the crest of the V+L surface is the pure H_2O boiling curve. At higher temperatures, the crest of the V+L surface is the critical curve, which defines a locus of pressure-temperature-salinity conditions at which liquid and vapor have identical properties. For a given temperature, the critical curve specifies the maximum pressure of vapor-liquid coexistence.

2. L: In the present context, L is a fluid with liquid-like properties in terms of density and enthalpy. In the single-phase domain at pressures above the V+L surface, fluid properties can continuously vary between vapor- and liquid-like without any heterogeneous phase change. Therefore, the distinction between liquid and vapor is based on convention, most commonly by defining fluids with a density less than that on the critical curve for the given salinity as vapor and those with a higher density as liquid. Liquid-like properties are generally encountered at high salinities, low temperatures, and high pressures within the single-phase domain.

3. V: Following the same convention, fluid in the single-phase domain exhibits vapor-like properties at low salinities, high temperatures, and low pressures. We use a slightly different, computationally pragmatic convention that defines "vapor" as a fluid with a salinity and pressure less than the critical values for a given temperature.

4. V+L+H: The vapor + liquid + halite surface forms the low-pressure boundary of V+L coexistence. The maximum pressure of V+L+H coexistence is ~39 MPa at ~595°C.

5. V+H: At pressures below the V+L+H surface, vapor coexists with solid halite.

6. L+H: The composition of halite-saturated liquid as a function of pressure and temperature is given by the halite liquidus. The low-pressure boundary of the halite liquidus is the V+L+H surface.

7. H: In our simulations, we observe precipitation of halite in sufficient quantities for it to nearly or even completely saturate the pore space. In the visualizations, we label the phase state H when the volumetric saturation of halite in the pore space exceeds 0.95 to highlight nearly complete clogging of pore space.

The term "supercritical" can only be defined by convention and strictly so only for one-component fluids (Liebscher and Heinrich, 2007). For dilute aqueous fluids, we define supercritical in relation to the temperature and enthalpy of the critical point of H_2O, irrespective of fluid pressure (see above**)**. In saline systems, such high-enthalpy, single-phase fluids are mostly restricted to the low-salinity, high-temperature part of the phase diagram.

The large-scale structure of a system driven by a shallow intrusion is shown in Figure 5a. Heated fluid ascends nearly vertically within an upflow plume (white areas), which show two-phase liquid-vapor (VL) zones extending to the depth of the intrusion. Fluid pressure above the intrusion is ~20 MPa (Figure 5a). Halite-saturated vapor (VH) forms around the intrusion at temperatures ≥400°C (Figure 5b) and is enveloped on the outside by a VL zone. Halite volumetric saturations exceed 0.95 above the center of the intrusion (H, purple area). Near the central base of the plume and overlying the VH zone, a heat pipe configuration with downflowing liquid and upflowing vapor develops (Figure 5b). While the salinity and density of liquid along the outer edge of the VL zone is ~3 wt % and ~600 kg m^{-3}, an increase to >25 wt % and 1000 kg m^{-3} at the base of VL zone above the H zone (Figure 5e), along with a low bulk fluid enthalpy of <1.5 MJ kg^{-1} (Figure 5c), indicates the accumulation of hypersaline brines at the base of the heat pipe zone.

A system with a deeper intrusion, emplaced at 4.5 km depth, shows vapor-rich upflow zones and, at fluid pressures >30 MPa near the intrusion, develops significant zones of phase separation by condensation (Figure 5f). In the deep parts, vapor saturation is >0.6 at the edge of the VL plume, and bulk fluid enthalpy is >2 MJ kg^{-1} (Figure 5h). Halite-saturated vapor develops at >500 °C and pressures below the maximum pressure of VH coexistence (~39 MPa), and is overlain by halite-undersaturated, single-phase vapor at the center of the upflow plume (Figure 5f). Halite zones are narrow and restricted to the margins of the VH zone (Figure 5g). The enthalpy of single-phase vapor above the center of the intrusion is >3 MJ kg^{-1}, and vapor saturation within the overlying VL zone is >0.7 (Figure 5h), thus implying that liquid is immobile. While bulk fluid salinity increases within the VL zone to >25 wt % at the boundary with the underlying VH zone, bulk fluid density is less than critical density of seawater (<454 kg m^{-3}) within the entire VL zone below 4 km depth (Figure 5j), an indication that the dominant mode of phase separation at these depths is condensation and that hypersaline brine does not accumulate in as large amounts as for the shallow system.

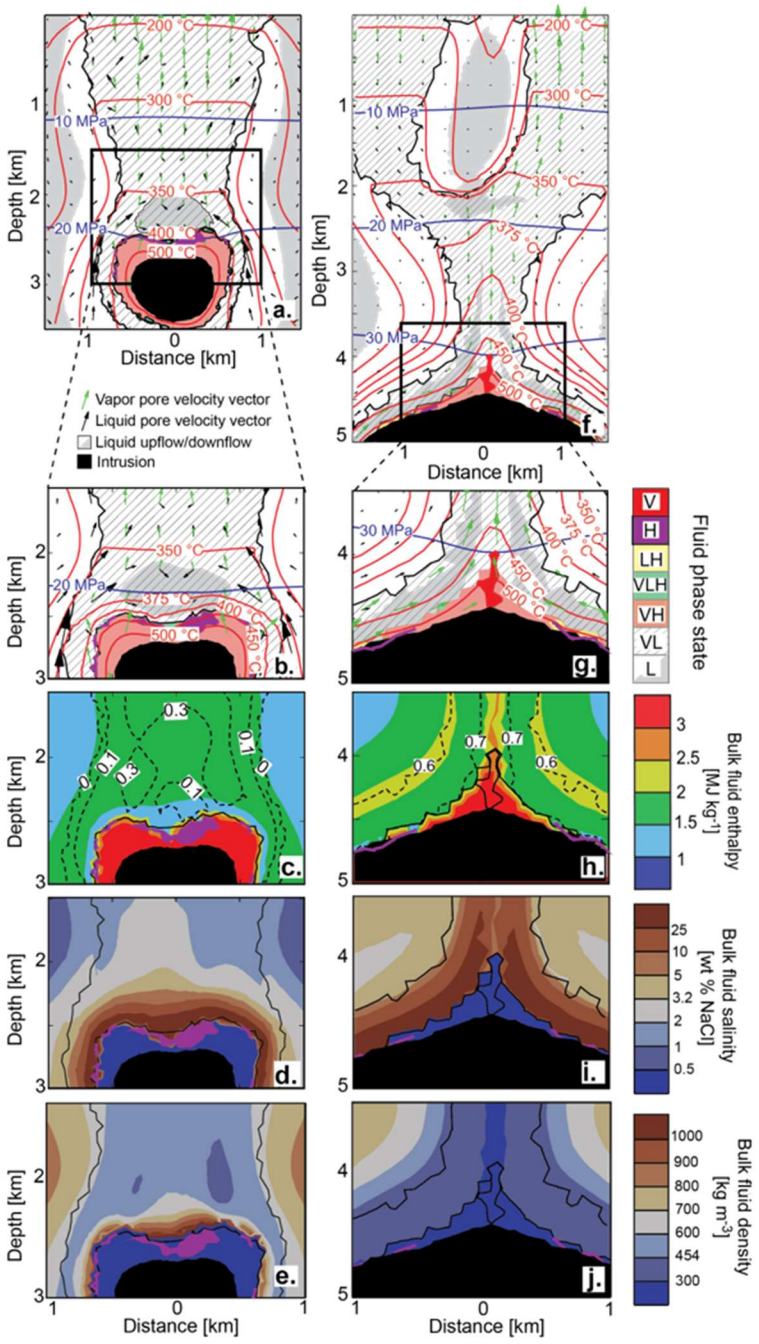

Figure 2: The thermal structure of saline geothermal systems. (a, f) Large-scale system structure for systems with shallow (2.5 km depth) or deep (4.5 km) intrusions after 3.6 and 7 ka of system evolution, respectively, are shown, with fluid phase state (see text), isotherms (red lines), isobars (blue lines), and liquid and vapor pore velocity vectors (black and green, respectively). Areas where the vertical component of the liquid flow is oriented upward or downward are colored in white or grey, respectively. The location of the intrusion, defined by having a permeability of $<10^{-16}$ m^2, is shown in black. Snapshots show the (b, g) fluid phase state, (c, h) vapor volumetric saturation (dashed lines) and bulk fluid enthalpy, (d, i) bulk fluid salinity, and (e, j) bulk fluid density. The area of the snapshots showing the excerpts in Figures (b–e) and (g–j) are shown by the black boxes in a and f (resp). Modified from Scott et al. (2017).

4. DISCUSSION

4.1 Characteristic Temperature Profiles, Natural Fluid Enthalpy Distribution and Depth of Boiling Zones

The simulations reveal characteristic temperature/depth profiles which allow a first-order diagnosis of host rock permeability and intrusion depth (Fig. 6a). Systems with high host rock permeability (blue lines) follow the boiling point curve to a maximum depth of 0.5–1 km, with the maximum depth of boiling decreasing as intrusion depth increases from 2–3 km. Temperatures in intermediate permeability systems (red lines) with intrusion depth ≤2.5 km follow the boiling point with depth curve over the entire depth range. In such systems,

temperatures are slightly elevated relative to the boiling point with depth curve (calculated for a column of pure vapor-saturated liquid) because fluid pressures are higher than hot hydrostatic. Fluid pressure gradients exceeding hot hydrostatic values are often measured in high-enthalpy geothermal systems (Donaldson et al., 1983).

Plotting the results in a pressure-enthalpy (*p-h*) diagram (Fig. 6b) explains the variations in geothermal system structure and depth of boiling and reveals that the upflow process is strongly non-isenthalpic. Systems display one of three general structures, with boiling restricted to the upper ~1 km, boiling from the surface down to the intrusion, or boiling underlain by hot supercritical fluid. Which structure a system shows results from an interplay between the input of hot supercritical fluid ascending from the intrusion, the brittle–ductile transition temperature, and the degree to which the rising fluid mixes with lower temperature fluids circulating near the intrusion. The enthalpy of ascending fluid decreases through fluid mixing and heat loss to the surroundings. Depending on how rapidly enthalpy decreases with depressurization, fluid passes from supercritical (red area) to two-phase conditions (blue area), or directly to a single-phase liquid (white area to the left of the liquid limb of the two-phase field). The former case results in vertically extensive boiling zones, while in the latter case, the paths intersect the liquid limb of the two-phase field at a lower pressure, producing boiling zones restricted to shallow depths (<1 km).

A rapid decrease in fluid enthalpy upon the onset of depressurization and fluid ascent produces shallow boiling zones restricted to shallow (<1 km) depth, as found in systems with high permeability and low T_{BDT} = 360 °C (Fig. 6b, blue path). Fluid enthalpy decreases from supercritical to <1.5 MJ kg^{-1} over a pressure range of a few MPa. Within the liquid field, enthalpy decreases more gradually, corresponding to near-isothermal ascent. The paths intersect the two-phase field at a pressure near ~5 MPa. Vertically extensive boiling zones are seen in systems with intermediate permeability (red paths) because fluid enthalpy at the onset of depressurization decreases more gradually into the two-phase field. High T_{BDT} increases the enthalpy of upflow zones by allowing the advection of supercritical fluid near the intrusion and variable mixing of this fluid with cooler waters during the process of ascent. Since fluid mixing is the main mechanism of enthalpy reduction and the extent of fluid mixing greatly depends on host rock permeability (Scott et al., 2015), high permeability systems develop somewhat lower enthalpies because the large fluxes of supercritical fluid are mixed with large quantities of recharging cooler liquid. In intermediate permeability systems, mixing is more stagnant and the enthalpy of the upflow is significantly higher. Furthermore, a deeper emplacement depth means a longer upflow path, and therefore a greater extent of fluid mixing and heat loss during fluid ascent.

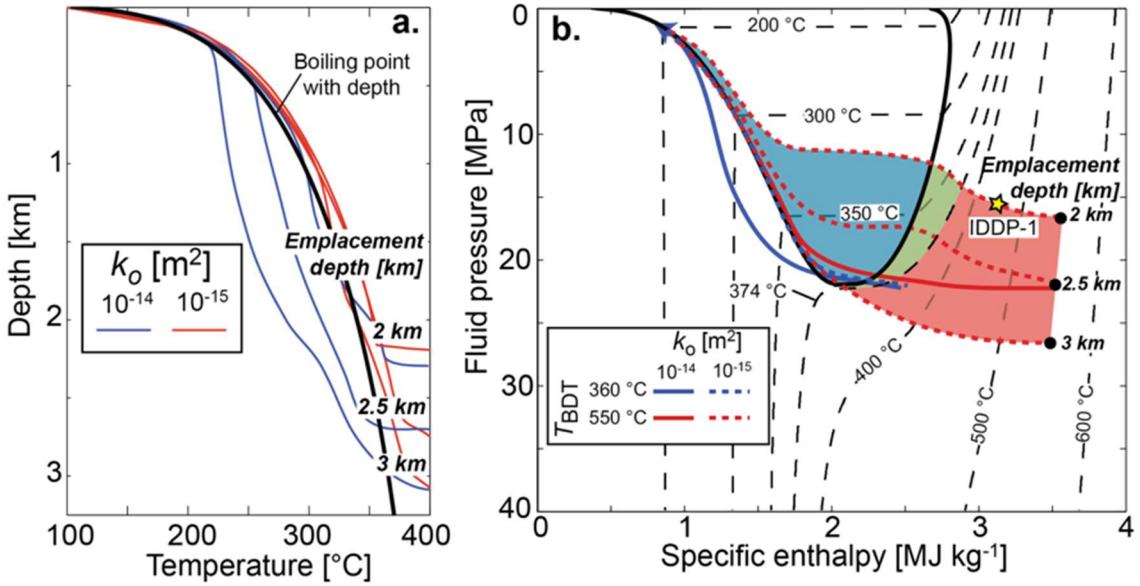

Figure 3: (a) Characteristic temperature-depth profiles resulting from variation of host rock permeability, emplacement depth, and brittle–ductile transition temperature of 360 °C. Red lines represent thermal conditions along the upflow path for systems with a permeability of 10^{-15} m^2, while blue lines show systems with a permeability of 10^{-14} m^2. (b) Pressure–enthalpy ascent paths superimposed onto a phase diagram of water. The areas of potentially exploitable supercritical fluid, single-phase vapor and two-phase fluid are shown in red, green, and blue, respectively. The measured reservoir temperature and enthalpy for the IDDP-1 well (450 °C, 3.2 MJ kg^{-1}, Axelsson et al., 2014) is shown with a yellow star. Modified from Scott et al. (2015).

4.2 Formation of Supercritical Geothermal Resources and Comparison with IDDP-1 Resource

Rocks which undergo the brittle-plastic transition at relatively high temperatures (>400 °C) allow the development of supercritical zones near the intrusion. In high permeability systems, the dilution of supercritical fluid ascending from the intrusion with large quantities of circulating liquid causes a rapid decrease in fluid temperature, and supercritical zones are restricted to narrow (~10 m thick) zones around the intrusion (Fig. 3d,f). Slower fluid circulation and less intense mixing in intermediate permeability systems leads to more spatially-extensive supercritical zones (Fig. 3e,g). For systems with high T_{BDT}, fluid enthalpy (Fig. 6b), rather than temperature, is a better gauge of the geologic controls and a better predictor of supercritical geothermal resources.

Our models explain the conditions encountered in the IDDP-1 well as the natural result of drilling into a shallow magmatic intrusion hosted in basaltic rock. The measured reservoir conditions (Fig. 6, yellow star) lie directly on the *p–h* ascent path of a system with a 2-km deep intrusion in rocks with T_{BDT} of 550 °C and an intermediate permeability of 10^{-15} m^2, values which are appropriate for the Krafla system (Violay et al., 2015; Bodvarsson et al., 1984). This correspondence corroborates our model results as well as the conclusion that supercritical geothermal resource properties depend on the primary geologic controls. The *p–h* relations further suggest that IDDP-1 drilled into a supercritical resource at close to the optimum conditions expected in the range of geologic parameters considered. Water at a similar temperature at greater depth would have a lower enthalpy, which might lead to unwanted liquid condensation upon near-isenthalpic depressurization during production from a wellbore but can be avoided if the specific enthalpy of the supercritical resource is greater than 2.8 MJ kg^{-1} (Fig. 6b). This highlights that, in contrast to previous thoughts, supercritical fluid pressures are not necessary for the development of economically attractive supercritical resources in systems with meteoric water.

4.3 Effect of Intrusion Depth on Style of Phase Separation and Heat Transport in Saline Geothermal Systems

Magma emplacement depth determines the hot-hydrostatic fluid pressure above an intrusion and thereby controls whether saline fluid circulating above an intrusion undergoes phase separation by boiling or condensation. Increasing intrusion emplacement depth from ~2.5 to 4.5 km shifts the hot-hydrostatic fluid pressure above an intrusion from values close to the critical pressure of pure water (Fig. 5a) to >30 MPa, close to the critical pressure of seawater (Figure 5f). While the boiling curve of pure water controls the maximum temperature of VL coexistence at pressures below the critical pressure of pure water, at higher pressures the maximum temperature of VL coexistence increases with increasing pressure along the H_2O-NaCl critical curve (Fig. 4). Therefore, heated seawater circulating near shallow intrusions will remain liquid-like and phase separate by boiling at pressures less than the critical pressure of seawater. At depths of >4 km, equivalent to hot-hydrostatic fluid pressures >30 MPa, seawater can be heated to >400 °C without undergoing phase separation, attain an intermediate, vapor-like density lower than the critical density of seawater (~450 kg m^{-3}; Figure 5j), and eventually phase separate by condensing small amounts of saline brine. Thus, fluids with seawater-like salinity will phase separate by boiling at low pressures above shallow intrusions and by condensation at high pressures above deep intrusions.

In the case of boiling, small fractions of low salinity vapor nucleate out of a liquid-like fluid upon phase separation (Fig. 4, blue lines). The low density of vapor causes it to ascend more rapidly than liquid in the buoyancy-driven convective field. Thus, vapor saturations are maintained at relatively low values in boiling zones above shallow intrusions. Two-phase heat pipes above the center of the intrusion are starved of less saline liquid, and low enthalpy hypersaline brines accumulate, descend, and precipitate halite as liquid is progressively boiled off. Although vapor enthalpy exceeds >3 MJ kg^{-1} around shallow intrusions, the near sealing of pore space resulting from the boiling of hypersaline brines greatly reduces the accessible enthalpy contained in the pore space, as well as rates of advective heat transport.

During condensation, a small fraction of low-enthalpy hypersaline brine condenses out of a high-enthalpy, vapor-like fluid (Figure 4, orange lines). Higher vapor saturations decrease the relative permeability of liquid and increase the relative permeability of vapor, thereby allowing higher vapor mass fluxes. Condensation may occur in two different settings: (1) along the outer edges of deep VL zones, where intermediate-density fluid with a salinity close to that of seawater is heated, and (2) the center of the upflow plume below the base of the VL zone, where low-salinity vapor ascending from underlying VH zones depressurizes. The latter settings have vapor saturations >0.7, which indicate that the liquid brine is an immobile wetting phase. Thus, advective heat transfer within condensation zones is dominated by vapor advection, and to a lesser extent, heat conduction through the rock, which boils off liquid and maintains near-residual liquid saturations (Figure 5h). Vertical vapor mass fluxes and advective heat transport are highest within VL condensation zones at temperatures near 400 °C, at which temperature the density of vapor is high (Klyukin et al., 2016).

The low mobility of dense, hypersaline brines at the base of the boiling plume reduces the effectiveness of convective heat loss from the top of shallow intrusions. The brine accumulation results from the downward liquid mass flux within the two-phase heat pipe at the base of the upflow plume (Figure 7a). At the interface with the underlying VH zone, liquid boils off to form solid halite and halite-saturated vapor. Upward liquid mass fluxes are maximized along the cooler edges of the VL plume, where groundwater with a salinity close to that of seawater can actively circulate. Similarly, upward vertical vapor mass fluxes are higher near the edges of the VL plume and relatively low within the two-phase heat pipe at the base of the VL zone (Figure 7b). While bulk fluid enthalpy and rates of advective heat transfer may exceed 3 MJ kg^{-1} and 50 W m^{-2} within the VH zone, such conditions occur only along the sides of the intrusion where halite saturations are low. Vapor mass fluxes and heat transfer are strongly reduced within the halite-rich part of the VH zone above the center of the intrusion (Figure 7c).

In contrast, vapor mass fluxes and rates of convective heat transfer are maximized within condensation zones above deep intrusions. Although these zones have lower liquid mass fluxes (Figure 7d), vapor mass fluxes are comparatively high and maximized within the center of the upflow plume, where vapor from the underlying VH zone ascends (Figure 7e). As a result of the high vapor mass fluxes, vertical convective heat fluxes throughout this area are >50 W m^{-2} (Figure 7f), in contrast to the generally lower values in shallower systems (Figure 7c). The IDDP-2 well recently drilled into the Reykjanes system was drilled to 4.5 km depth and encountered a bottom-hole temperature of 426 ºC and fluid pressure of 34 MPa (Friðleifsson et al., 2017). While these temperature and pressure conditions are sufficient for the development of a condensation zone, whether this reservoir is indeed undergoing active condensation and will sustain high rates of fluid production depends on permeability and proximity to a magmatic intrusion, among other factors.

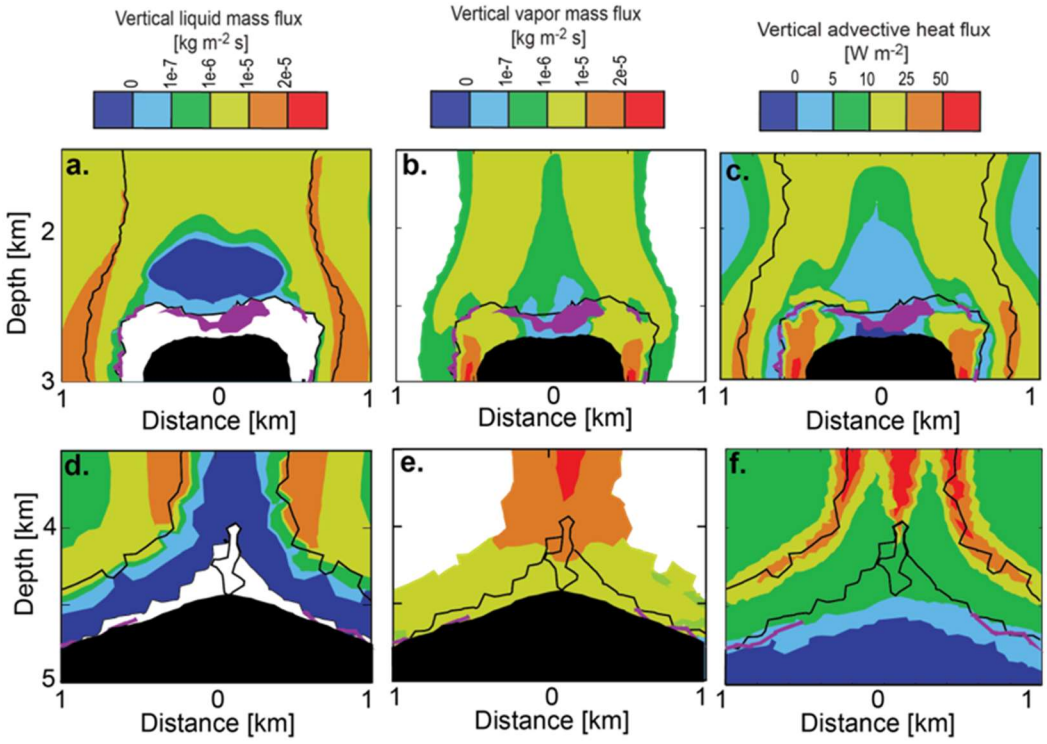

Figure 7: Vertical liquid and vapor and advective heat fluxes by thermohaline convection above intrusions. Snapshots show the (a, d) distribution of vertical liquid mass fluxes, (b, e) vertical vapor mass fluxes, (c, f) vertical advective heat flux for systems with (Figures 5a–e) shallow or (Figures 5f–h) deep intrusion emplacement depth. The intrusion is shown in black, and halite zones (see text) are shown in purple. Modified from Scott et al. (2017).

5. CONCLUSIONS

This study presents generic numerical simulations used to identify first-order geologic controls on the of high-enthalpy, magma-driven geothermal systems. New insights emerging out of this work include:

- Host rock permeability is a primary control on the depth and general structure of boiling zones, as systems with high permeability (10^{-14} m^2) show shallow boiling zones generally restricted to <1 km depth, while intermediate permeability systems (10^{-15} m^2) display vertically extensive boiling zones reaching from the surface to the intrusion.
- An initially symmetrical model set-up generates chaotic, asymmetrical upflow plumes.
- Boiling at shallow depths continues for many thousands of years after an intrusive heat source has cooled.
- A new and practical definition of supercritical geothermal resources based on fluid specific enthalpy, temperature and rock permeability accounts for the development economically-attractive supercritical resources above shallow intrusions, where hot-hydrostatic fluid pressure is less than the critical pressure of pure water (as was the case for the IDDP-1 resource).
- Non-isenthalpic fluid upflow generates conventional geothermal resources overlying supercritical zones through the mixing of supercritical fluids ascending from the intrusion and cooler circulating fluids.
- The style of fluid phase separation near the intrusion exercises a first-order control on the dynamics and efficiency of heat and mass transfer. Phase separation above shallow intrusions (~2 km) is carried out though boiling and leads to accumulation of low-mobility hypersaline brines and halite precipitation, thereby reducing the efficiency of heat and mass transfer.
- Above deeper intrusions (4 km), phase separation occurs by condensation of hypersaline brine from intermediate-density (vapor-like) fluid. Since the fraction of brine remains small, advective, vapor-dominated mass and heat fluxes are maximized. Thus, in contrast to pure water systems, for which shallow intrusions were deemed to make better targets for supercritical resource exploitation, the optimal targets in saline systems are located above deeper intrusions.

In the future, CSMP++ will be used for geologically more complex, site-specific geometries. These analyses can be compared against geophysical data and well measurements to both gain confidence in model results and maximize their usefulness as exploration tools.

6. ACKNOWLEDGEMENTS

We thank the COTHERM partners, particularly Andri Stefánsson, Melchior Grab, Matylda Hermanska, Dimitri Kulik, Bruno Thein, Stuart Greenhalgh, and Hansruedi Maurer. This manuscript benefited from fruitful discussions with Matthew Steele-MacInnis, Pilar Lecumberri-Sanchez and Szandra Fekete. This study was funded by the Swiss National Science Foundation [grant number CRSII2 141843/1, Sinergia COTHERM].

7. DATA AVAILABILITY

Unprocessed model output data will be provided as zipped archives in an online repository. The CSMP++ computing platform is co-owned by ETH Zurich, Heriot Watt University, and Montanuniversität Leoben. Source code is not distributed freely; precompiled code libraries may be obtained via one of the owning institutions.

8. REFERENCES

Axelsson, G., Egilson, T. and Gylfadóttir, S.: Modelling of temperature conditions near the bottom of well IDDP-1 in Krafla, Northeast Iceland. *Geothermics,* **49**, (2014), 49–57.

Bödvarsson, G., Lippmann, M.J. and Pruess, K.: Modeling of Geothermal Systems, *Journal of Petroleum Technology,* **38**, (1986), 1007-1021

Bödvarsson, G., Pruess, K., Stefánsson, V. and Eliasson, E.: The Krafla geothermal field, Iceland 2. The natural state of the system, *Water Resources Research,* **20**, (1984), 1531–1544.

Cathles, L.M.: An Analysis of the Cooling of Intrusives by Ground-Water Convection Which Includes Boiling, *Economic Geology,* **72**, (1977), 804–826.

Cathles, L., Erendi, A., and Barrie, T.: How long can a hydrothermal system be sustained by a single intrusive event?, *Economic Geology,* **92**, (1997), 766–771.

Cumming, W.: Geophysics and resource conceptual models in geothermal exploration and development*, Geothermal Power Generation* (ed. R. DiPippo)*,* Woodhead Publishing, (2016).

Donaldson, I., Grant, M. and Bixley, P.: Nonstatic Reservoirs: The Natural State of the Geothermal Reservoir, *Journal of Petroleum Technology,* **35**, (1983), 189–194.

Driesner, T.: The system H_2O-NaCl. Part II: Correlations for molar volume, enthalpy, and isobaric heat capacity from 0 to 1000 °C, 1 to 5000 bar, and 0 to 1 X_{NaCl}, *Geochimica Cosmochimica Acta,* **71**, (2007), 4902–4919.

Driesner, T. and Heinrich, C.A.: The system H_2O–NaCl. Part I: Correlation formulae for phase relations in temperature–pressure–composition space from 0 to 1000 °C, 1 to 5000 bar, and 0 to 1 X_{NaCl}, *Geochimica Cosmochimica Acta,* **71**, (2007), 4880–4901.

Elders, W.A., Friðleifsson, G.Ó. and Albertsson, A.: Drilling into magma and the implications of the Iceland Deep Drilling Project (IDDP) for high-temperature geothermal systems worldwide, *Geothermics,* **49**, (2014), 111–118.

Fournier, R.: Conceptual Models of Brine Evolution in Magmatic-Hydrothermal Systems, *Volcanism in Hawaii*, (1987), 1487–1506.

Fournier, R.: Hydrothermal Processes Related to Movement of Fluid from Plastic into Brittle Rock in the Magmatic-Epithermal Environment, *Economic Geology,* **94**, (1999), 1193–1210.

Foustoukos, D. I. and Seyfried, W.E.: Fluid Phase Separation Processes in Submarine Hydrothermal Systems, *Reviews in Mineralogy and Geochemistry,* **65**, (2007), 213–239.

Friðleifsson, G. Ó., Elders, W.A. and Albertsson, A.: The concept of the Iceland deep drilling project, *Geothermics,* **49**, (2014), 2–8.

Friðleifsson, G. Ó., Elders, W.A., Zierenberg, R.A., Stefánsson, A., Fowler, A.P.G., Weisenberger, T.B., Harðarson, B.S., and Mesfin, K.G.: The Iceland Deep Drilling Project 4.5 km deep well, IDDP-2, in the seawater-recharged Reykjanes geothermal field in SW Iceland has successfully reached its supercritical target, *Scientific Drilling,* **23**, (2017), 1–12.

Geiger, S., Driesner, T., Heinrich, C. and Matthäi, S.K.: On the dynamics of NaCl-H_2O fluid convection in the Earth's crust, *Journal of Geophysical Research,* **110**, (2005), B07101.

Grant, M.A., and Bixley, P.F.: *Geothermal Reservoir Engineering*, Second Edition, Academic Press, (2011).

Haar, L., Gallagher, J.S., and Kell, G.: *NBS/NRC steam tables*, Hemisphere Publishing, Washington D.C., (1984).

Hayba, D.O., and Ingebritsen, S.E.: Multiphase groundwater flow near cooling plutons, *Journal of Geophysical Research,* **102**, (1997), 12235.

Ingebritsen, S.E., and Hayba, D.O.: Fluid Flow and Heat Transport Near the Critical Point of H_2O, *Geophysical Research Letters,* **21**, (1994), 2199-2202.

Ingebritsen, S.E., Sanford, W., and Neuzil, C.E.: *Groundwater in Geologic Processes*, Second Edition, Cambridge University Press, New York, (2006).

Jupp, T. and Schultz, A.: A thermodynamic explanation for black smoker temperatures, *Nature,* **403**, (2000), 880–3.

Klyukin, Y., Driesner, T., Steele-MacInnis, M., Lowell, R.P., and Bodnar, R.J.: Effect of salinity on mass and energy transport by hydrothermal fluids based on the physical and thermodynamic properties of H_2O-NaCl, *Geofluids*, **16**, (2016), 585-603.

Liebscher, A., and Heinrich, C.A.: Fluid-Fluid Interactions in the Earth's Lithosphere, *Reviews in Mineralogy and Geochemistry,* **65**, (2007), 1–13.

Norton, D., and Knight, J.: Transport Phenomena in Hydrothermal Systems: Cooling Plutons, *American Journal of Science,* **277**, (1977) , 937–981.

O'Sullivan, M.J., Pruess, K., and Lippmann M.J.: State of the art of geothermal reservoir simulation, *Geothermics,* **30**, (2001), 395–429.

Pritchett, J.W.: Geothermal Reservoir Engineering in the United States Since the 1980's, *GRC Transactions,* **31**, (2007) 31–37.

Reinsch, T., Dobson, P., Asanuma, H., et al. "Utilizing Supercritical Geothermal Systems: A Review of Past Ventures and Ongoing Research Activities." *Geothermal Energy,* **5**, (2017).

Scott S., Driesner, T., and Weis, P.: Geologic controls on supercritical geothermal resources above magmatic intrusions, *Nature Communications,* **6**, (2015), 7837.

Scott, S., Driesner, T., and Weis, P.: The thermal structure and temporal evolution of high-enthalpy geothermal systems, *Geothermics,* **62**, (2016), 33–47.

Scott, S., Driesner, T., and Weis, P.: Boiling and condensation of saline geothermal fluids above magmatic intrusions, *Geophysical Research Letters,* **44**, (2017), 1–10.

Violay, M., Gibert, B., Mainprice, D. and Burg, J.-P.: Brittle versus ductile deformation as the main control of the deep fluid circulation in oceanic crust, *Geophysical Research Letters,* **42**, (2015).

Weis, P., Driesner, T., Coumou, D. and Geiger, S.: Hydrothermal, multiphase convection of H_2O-NaCl fluids from ambient to magmatic temperatures: a new numerical scheme and benchmarks for code comparison, *Geofluids,* **14**, (2014), 347–371.